

## An Improved Calibration of the Wavelength Dependence of Metallicity on the Cepheid Leavitt law

LOUISE BREUVAL,<sup>1,2</sup> ADAM G. RIESS,<sup>1,3</sup> AND PIERRE KERVELLA<sup>2</sup>

<sup>1</sup>*Department of Physics and Astronomy, Johns Hopkins University, Baltimore, MD 21218, USA*

<sup>2</sup>*LESIA, Observatoire de Paris, Université PSL, CNRS, Sorbonne Université, Université de Paris, 5 place Jules Janssen, 92195 Meudon, France*

<sup>3</sup>*Space Telescope Science Institute, 3700 San Martin Drive, Baltimore, MD 21218, USA*

(Received ...; Revised ...; Accepted ...)

### ABSTRACT

The Cepheid period-luminosity (PL) relation (or Leavitt law) has served as the first rung of the most widely used extragalactic distance ladders and is central to the determination of the local value of the Hubble constant ( $H_0$ ). We investigate the influence of metallicity on Cepheid brightness, a term that significantly improves the overall fit of the distance ladder, to better define its wavelength dependence. To this aim, we compare the PL relations obtained for three Cepheid samples having distinct chemical composition (in the Milky Way and Magellanic Clouds) and focusing on the use of improved and recent data while covering a metallicity range of about 1 dex. We estimate the metallicity effect (hereafter  $\gamma$ ) in 15 filters from mid-infrared to optical wavelengths, including 5 Wesenheit indices, and we derive a significant metallicity term in all filters, in accord with recent empirical studies and models, in the sense of metal-rich Cepheids being brighter than metal-poor ones. We describe the contribution of various systematic effects in the determination of the  $\gamma$  term. We find no evidence of  $\gamma$  changing over the wavelength range  $0.5 - 4.5 \mu\text{m}$  indicating the main influence of metallicity on Cepheids is in their luminosity rather than color. We identify factors which sharpen the empirical constraints on the metallicity term over past studies including corrections for the depth of the Magellanic Clouds, better calibrated Cepheid photometry, improved Milky Way extinction estimates and revised and expanded metallicity measurements in the LMC.

### 1. INTRODUCTION

The Cepheid period-luminosity (PL) relation (or Leavitt law, [Leavitt & Pickering 1912](#)) is a fundamental tool for measuring astronomical distances and has been used for decades to estimate the current expansion rate of the Universe, the Hubble constant ([Freedman et al. 2001](#); [Riess et al. 2022](#)). Recently, a significant tension of  $5\sigma$  has arisen between the prediction of  $H_0$  from the Cosmic Microwave Background (CMB) data from [Planck Collaboration et al. \(2020\)](#) assuming a  $\Lambda$ CDM model,  $H_0 = 67.4 \pm 0.5 \text{ km s}^{-1} \text{ Mpc}^{-1}$ , and its empirical estimate based on Cepheids and SNe Ia measurements,  $H_0 = 73.04 \pm 1.04 \text{ km s}^{-1} \text{ Mpc}^{-1}$  ([Riess et al. 2022](#)). The persistence of this discrepancy could have significant im-

plications in cosmology as it may suggest a breach in the standard model ([Di Valentino et al. 2021](#)). It is therefore important to empirically scrutinize the nature of the Leavitt Law.

In the present paper, we aim at measuring the influence of chemical abundance on Cepheid brightness, as this term has been found to significantly improve the quality of the fit of the distance ladder. The difference in metallicity between Cepheids used to calibrate the PL relation and Cepheids in SNe Ia host galaxies is usually taken into account by including a corrective term ( $\gamma$ ) in the PL relation, such that:

$$M = \alpha (\log P - \log P_0) + \delta + \gamma [\text{Fe}/\text{H}] \quad (1)$$

The majority of extragalactic Cepheids in SN Ia hosts have inferred abundances that are similar to those in two distance ladder anchors, the Milky Way (MW)

and NGC 4258, in terms of metal content (see Fig. 21 in [Riess et al. 2022](#)). However, the Large Magellanic Cloud (LMC) which contains more metal-poor Cepheids, is also often used as an anchor in the distance ladder: its distance was measured with high precision by [Pietrzyński et al. \(2019\)](#) using detached eclipsing binaries (DEBs). The improved characterization of the distance ladder depends on an improved constraint on the metallicity term to span such a range of metallicity. The best accuracy on this term can thus be obtained by using an even larger metallicity range including the even more metal poor Small Magellanic Cloud (SMC) and its recently measured DEB distance ([Graczyk et al. 2020](#)).

Various estimates of the metallicity effect were published in the last two decades, based on different methods, samples, photometry, distances or chemical abundances. They are listed in Table 1. Early studies using nonlinear convecting models ([Bono et al. 1999, 2008](#); [Caputo et al. 2000](#); [Marconi et al. 2005](#)) based on masses and luminosities provided by stellar evolutionary calculations predicted a positive metallicity effect ( $\gamma > 0$ ), meaning that metal-rich Cepheids are fainter than metal-poor ones. A positive metallicity term might be explained as a strictly atmospheric effect from line blanketing with higher metallicity producing more absorption lines to decrease the flux emitted by the star and make it appear fainter than expected in the optical ([Freedman & Madore 2011](#)), although this explanation does not address possible changes to a Cepheid’s bolometric luminosity. More recently, [Anderson et al. \(2016\)](#) used stellar models from the Geneva group including the effects of shellular rotation and derived a strong negative dependence in the optical and NIR (see Sect. 5.4), meaning that metal-rich Cepheids would be brighter.

On the other hand, almost all recent empirical studies have obtained a negative metallicity term ( $\gamma < 0$ ) based on extragalactic Cepheids ([Macri et al. 2006](#); [Scowcroft et al. 2009](#)), Baade-Wesselink distances of Milky Way and Magellanic Cloud Cepheids ([Storm et al. 2011a](#); [Groenewegen 2013](#); [Gieren et al. 2018](#)), DEB distances for Magellanic Cloud Cepheids ([Wielgórski et al. 2017](#)), Gaia DR2 or EDR3 parallaxes ([Groenewegen 2018](#); [Ripepi et al. 2020, 2021](#); [Riess et al. 2021](#)). [Romaniello et al. \(2008\)](#) provided a range of metal abundances of individual LMC Cepheids which were used by [Freedman & Madore \(2011\)](#) to derive a negative metallicity term in the mid-infrared (MIR) *Spitzer* bands, becoming progressively weaker and then positive towards op-

tical wavelengths, with a crossover around the near infrared (NIR). However, a significant revision as well as an expansion of these measurements by [Romaniello et al. \(2022\)](#) concluded there was no significant differences among the individual metallicities of LMC Cepheids, negating the ability to constrain the metallicity term internal to the LMC. Non-trivial depth of the Magellanic Clouds is also an important factor as the scale of the metallicity term between the Clouds and the Milky Way is  $< 0.1$  mag.

Improving data quality necessitates a study of the metallicity term outside the context of the distance ladder and over a broader range of wavelength. Because the accuracy required to resolve the metallicity term, a few hundredths of a magnitude, is comparable to historic zeropoint errors, consistent calibration of Cepheid photometry is paramount. While the distance ladder combines constraints on the metallicity term from both metallicity gradients within hosts and abundance differences between hosts ([Riess et al. 2022](#)), we focus here on the constraints from the latter as these offer the best combination of simplicity, wavelength coverage and constraining power.

In [Breuval et al. \(2021\)](#) (hereafter [B21](#)), we calibrated  $\gamma$  in 7 ground-based filters covering NIR and optical wavelengths, including two Wesenheit indices. The present work aims at improving, expanding and complementing this preliminary study with new data, in particular by including two additional mid-infrared (MIR) *Spitzer* bands, three additional optical *Gaia* bands as well as three supplementary Wesenheit indices (including the HST reddening-free  $W_H$  band used in the SH0ES papers, e.g. [Riess et al. 2022](#)), resulting in a total of 15 different filters. The large wavelength coverage ( $0.5 < \lambda < 4.5 \mu\text{m}$ ) also allows for a study of a possible dependence between  $\gamma$  and  $\lambda$ . Following [B21](#), we adopt three Cepheid samples of different chemical abundance which also have precise distances: Milky Way, LMC and SMC Cepheids. Sect. 2 describes the data used in this analysis. The method is outlined in Sect. 3 and the results are given in Sect. 4. We discuss our findings in Sect. 5 and conclude with perspectives in Sect. 6.

## 2. DATA

This section describes the catalogs used in this analysis (photometry, reddenings, distances and metallicities), they are listed in Table 2.

**Table 1.** Empirical and theoretical estimates of the metallicity effect ( $\gamma$  in mag/dex) on Cepheid brightness.

Band	$\gamma$	Reference	Method	
<b>THEORETICAL STUDIES</b>				
$V$	+0.40	Bono et al. (1999)	Nonlinear convecting models	[Fe/H]
$K$	-0.08			
$W_{VI}$	+0.27	Caputo et al. (2000)	Nonlinear convecting models	[Fe/H]
$W_{VI}$	$\gamma > 0$	Marconi et al. (2005)	Nonlinear convecting models	[Fe/H]
$W_{VI}$	+0.05 $\pm$ 0.03	Bono et al. (2008)	Nonlinear convecting models	[Fe/H]
$V$	-0.277 $\pm$ 0.102	Anderson et al. (2016)	Geneva evolution models including	
$H$	-0.214 $\pm$ 0.086		the effects of rotation (2 <sup>nd</sup> crossing),	
$W_{VI}$	-0.221 $\pm$ 0.097		average between blue and red edge	
$W_H$	-0.205 $\pm$ 0.084			
<b>EMPIRICAL STUDIES</b>				
$W_{VI}$	-0.24 $\pm$ 0.16	Kennicutt et al. (1998)	2 fields in M101	[O/H]
$W_{VI}$	-0.24 $\pm$ 0.05	Sakai et al. (2004)	TRGB/Cepheid distances to nearby galaxies	[O/H]
$W_{VI}$	-0.29 $\pm$ 0.10	Macri et al. (2006)	2 fields in NGC 4258	[O/H]
$K$	$\sim 0$	Romaniello et al. (2008)	MW, LMC, SMC + HR spectra	[Fe/H]
$V$	$\gamma > 0$			
$W_H$	-0.23 $\pm$ 0.17	Riess et al. (2009)	HST photometry, NGC 4258	[O/H]
$W_{VI}$	-0.29 $\pm$ 0.11	Scowcroft et al. (2009)	4 fields in M33	[O/H]
$W_H$	-0.10 $\pm$ 0.09	Riess et al. (2011)	HST photometry, MW, LMC, NGC 4258	[O/H]
$V$	+0.50 $\pm$ 0.31	Freedman & Madore (2011)	Abundances of individual LMC Cepheids	[Fe/H]
$J$	+0.14 $\pm$ 0.07			
$H$	+0.05 $\pm$ 0.02			
$K$	+0.02 $\pm$ 0.03			
[3.6 $\mu$ m]	-0.39 $\pm$ 0.16			
[4.5 $\mu$ m]	-0.25 $\pm$ 0.18			
[5.8 $\mu$ m]	-0.39 $\pm$ 0.17			
[8.0 $\mu$ m]	-0.38 $\pm$ 0.16			
[3.6 $\mu$ m]	-0.09 $\pm$ 0.29	Freedman et al. (2011)	MW, LMC, SMC	[Fe/H]
$V$	+0.09 $\pm$ 0.10	Storm et al. (2011a)	MW, LMC, SMC + IRSB BW distances	[Fe/H]
$I$	-0.06 $\pm$ 0.10		$p = 1.55 - 0.186 \log P$	
$W_{VI}$	-0.23 $\pm$ 0.10		(Storm et al. 2011b)	
$J$	-0.10 $\pm$ 0.10			
$K$	-0.11 $\pm$ 0.10			
$W_{JK}$	-0.10 $\pm$ 0.10			
$V$	+0.23 $\pm$ 0.11	Groenewegen (2013)	MW, LMC, SMC + IRSB BW distances	[Fe/H]
$K$	-0.05 $\pm$ 0.10		$p = 1.50 - 0.24 \log P$	
$W_{VK}$	+0.04 $\pm$ 0.10			
$W_H$	-0.14 $\pm$ 0.06	Riess et al. (2016)	HST photometry, MW, LMC, NGC 4258	[O/H]
$V$	-0.022 $\pm$ 0.076	Wielgórski et al. (2017)	LMC, SMC + DEB distances	[Fe/H]
$I$	-0.015 $\pm$ 0.071			
$J$	-0.042 $\pm$ 0.069			
$H$	-0.012 $\pm$ 0.069			
$K$	-0.017 $\pm$ 0.069			
$W_{VI}$	-0.025 $\pm$ 0.067			
$W_{JK}$	-0.022 $\pm$ 0.067			
$V$	-0.238 $\pm$ 0.186	Gieren et al. (2018)	MW, LMC, SMC + IRSB BW distances	[Fe/H]
$I$	-0.293 $\pm$ 0.150		$p = 1.55 - 0.186 \log P$ (Storm et al. 2011b)	

**Table 1** (continued)

Band	$\gamma$	Reference	Method
$W_{VI}$	$-0.335 \pm 0.059$		
$J$	$-0.270 \pm 0.108$		
$K$	$-0.232 \pm 0.064$		
$W_{JK}$	$-0.221 \pm 0.053$		
$V$	$-0.041 \pm 0.260$	Groenewegen (2018)	MW <i>Gaia</i> DR2 parallaxes, ZP = $-0.046$ mas [Fe/H]
$K$	$-0.168 \pm 0.146$		
$W_{VK}$	$-0.188 \pm 0.142$		
$W_H$	$-0.17 \pm 0.06$	Riess et al. (2019)	HST photometry, MW, LMC, NGC 4258 [O/H]
$K$	$-0.082 \pm 0.138$	Ripepi et al. (2020)	MW <i>Gaia</i> DR2 parallaxes, ZP = $-0.049$ mas [Fe/H]
$W_{JK}$	$-0.284 \pm 0.115$		
$K$	$-0.456 \pm 0.099$	Ripepi et al. (2021)	MW <i>Gaia</i> EDR3 parallaxes + HR spectra [Fe/H]
$W_{JK}$	$-0.465 \pm 0.071$		
$W_{VK}$	$-0.459 \pm 0.107$		
$V$	$-0.048 \pm 0.055$	Breuval et al. (2021)	MW, LMC, SMC [Fe/H]
$I$	$-0.138 \pm 0.053$		<i>Gaia</i> EDR3 parallaxes + DEB distances
$W_{VI}$	$-0.251 \pm 0.057$		
$J$	$-0.208 \pm 0.052$		
$H$	$-0.152 \pm 0.092$		
$K$	$-0.221 \pm 0.051$		
$W_{JK}$	$-0.214 \pm 0.057$		
$W_H$	$-0.217 \pm 0.046$	Riess et al. (2022)	Cepheids with HST/WFC3 photometry [O/H]

### 2.1. Photometry

In order to minimize systematic uncertainties related to the use of disparate photometric systems present in many literature compilations of Cepheid magnitudes, we adopt the most homogeneous and consistently calibrated data sets available, while ensuring at the same time that the best light curve coverage is obtained for the Cepheids.

**NIR ground  $J$ ,  $H$  and  $K$  filters:** in the NIR, we adopted the photometry from Monson & Pierce (2011) transformed in the 2MASS system for MW Cepheids. Mean magnitudes of LMC Cepheids are taken from the Synoptic Survey by Macri et al. (2015) (hereafter M15) which also includes additional Cepheids from Persson et al. (2004). Finally, the VISTA survey for the Magellanic Clouds (VMC) by Ripepi et al. (2016) provides  $J$  and  $K$  band light curves for a large number of SMC Cepheids. We complemented these data with the  $H$  band single epoch photometry from the Kato et al. (2007) Point Source Survey. Empirically-derived transformations for zeropoints and color terms are applied to bring LMC and SMC NIR photometry to match the 2MASS system, the details can be found in Sect. 2.2 and 2.3 in B21.

**Optical ground  $V$  and  $I$  filters:** in the  $V$  and  $I$  bands, we adopt the compilation of light curves from Berdnikov (2008) for MW Cepheids. In the LMC and SMC, we adopt the OGLE-IV survey from Soszyński et al. (2015), combined with the Shallow Survey of bright LMC Cepheids by Ulaczyk et al. (2013). For consistency, we select the list of Cepheids from Macri et al. (2015) for the LMC sample. We note the lack of a more consistently calibrated, modern set of all-sky optical Cepheid data for the Milky Way sample, making it the most limiting dataset in the following studies.

***Gaia* optical  $G$ ,  $BP$  and  $RP$  filters:** We used the intensity averaged mean magnitudes provided in the *Gaia* DR2 "vari\_cepheid" catalog by Clementini et al. (2019) in the three optical *Gaia* bands, for Milky Way, LMC and SMC Cepheids. When the errors on apparent mean magnitudes are smaller than 0.001 mag, we set them to 0.010 mag. No updates to this were available in EDR3. These are internally photometrically consistent.

***Spitzer* mid-infrared [3.6  $\mu\text{m}$ ] and [4.5  $\mu\text{m}$ ] filters:** A sample of 37 Galactic Cepheids were observed with the *Spitzer* Space Telescope, their mean magnitudes are provided in the mid-infrared [3.6  $\mu\text{m}$ ] and [4.5  $\mu\text{m}$ ] filters by Monson et al. (2012). Similarly, 85

**Table 2.** References for the data adopted in this study.

	Milky Way	Large Magellanic Cloud	Small Magellanic Cloud
$V, I$	Berdnikov (2008)	Soszyński et al. (2015) Ulaczyk et al. (2013)	Soszyński et al. (2015)
$J, H, K$	Monson & Pierce (2011)	Macri et al. (2015) Persson et al. (2004)	$J, K$ : Ripepi et al. (2016) $H$ : Kato et al. (2007)
$G, BP, RP$	Clementini et al. (2019)	Clementini et al. (2019)	Clementini et al. (2019)
$[3.6 \mu\text{m}], [4.5 \mu\text{m}]$	Monson et al. (2012)	Scowcroft et al. (2011)	Scowcroft et al. (2016)
$F160W, F555W, F814W$	Riess et al. (2021)	Riess et al. (2019)	–
Reddening	(a) Bayestar dust map (Green et al. 2019) (b) Period-color relation (Riess et al. 2022) (c) SPIPS method (Trahin et al. 2021)	Skowron et al. (2021) reddening maps	Skowron et al. (2021) reddening maps
Distance	Bailer-Jones et al. (2021) distances (includes ZP correction by Lindegren et al. (2021)) + additional ZP of 0.014 mas (Riess et al. 2021)	DEB distance $49.59 \pm 0.09 \pm 0.54$ kpc (Pietrzyński et al. 2019) + geometry correction	DEB distance $62.44 \pm 0.47 \pm 0.81$ kpc (Graczyk et al. 2020) + geometry correction
Metallicity	Genovali et al. (2014, 2015) and references therein $[\text{Fe}/\text{H}] = +0.085 \pm 0.022$ dex	Romaniello et al. (2022) $[\text{Fe}/\text{H}] = -0.407 \pm 0.020$ dex	Gieren et al. (2018) $[\text{Fe}/\text{H}] = -0.75 \pm 0.05$ dex

LMC Cepheid and 90 SMC Cepheid mean magnitudes were measured in the same filters by Scowcroft et al. (2011) and Scowcroft et al. (2016) respectively. These are internally photometrically consistent.

**Hubble Space Telescope (HST) Wide Field Camera 3 (WFC3) filters:** The HST WFC3 filters  $F555W$ ,  $F814W$  and  $F160W$  are particularly interesting since they can be combined into the reddening-free Wesenheit index  $W_H$ , which is also used to observe extragalactic Cepheids (Riess et al. 2022), cancelling photometric zero-point errors on the distance scale. Riess et al. (2021) provides HST/WFC3 photometry for 75 Milky Way Cepheids obtained by the spatial scanning technique. Similarly, Riess et al. (2019) measured HST/WFC3 mean magnitudes in the same filters for 70 LMC Cepheids. Unfortunately, there is currently no available HST photometry for SMC Cepheids: in the HST photometric system, the analysis will be limited to Galactic and LMC Cepheids only.

**Systematic uncertainties:** In  $V$ ,  $I$ ,  $J$ ,  $H$  and  $K$ , the photometry for Galactic and Magellanic Cloud Cepheids was obtained with different instruments and sometimes in different systems (see Table 2): we include an error of 0.020 mag to the PL intercepts in these five filters for each host. For *Gaia*, *Spitzer* and *HST* photometry, the data are taken with the same instruments and reduced by the same teams for the 3 galaxies so they do not require any systematic zeropoint uncertainty.

Additionally, the Berdnikov (2008) catalog gathers observations made between 1986 and 2004 which are rather inhomogeneous, therefore we include quadratically an additional photometric zero-point uncertainty of 0.010 mag for MW Cepheids in  $V$  and  $I$ , which sums to a total systematic zeropoint difference between Cepheids in the MW and either Cloud of  $\sigma = 0.03$  mag in these bands. For the LMC sample, M15 reports zero-point differences of  $0.018 \pm 0.067$ ,  $-0.016 \pm 0.058$  and  $0.000 \pm 0.054$  mag in  $J$ ,  $H$ ,  $K$  respectively between M15 and Persson et al. (2004), after transformation into the 2MASS system. We adopt these values as photometric zero-point error in the NIR for LMC Cepheids to account for the internal consistency of the M15 catalog. Finally, from the comparison between Kato et al. (2007) and VMC magnitudes in the SMC, a photometric zero-point uncertainty of 0.010 mag is adopted in the  $J$ ,  $H$ ,  $K$  bands for the Cepheids of this galaxy.

## 2.2. Reddening

Apparent magnitudes must be carefully corrected for extinction, due to the presence of dust on the line of sight, using a reddening law and consistent  $E(B-V)$  values. Past studies have relied on the Fernie et al. (1995) database which is an inhomogeneous compilation of major colour excess determinations published since 1975 derived from 17 sources of mostly photoelectric data in non-standard bandpass systems and which are therefore inadequate for providing consistent reddening estimates

**Table 3.** Filters in which the effect of metallicity is calibrated in this study: effective central wavelength ( $\lambda_0^{\text{eff}}$ ), ratios of total-to-selective absorption ( $R_\lambda$ ) from Wang & Chen (2019) assuming  $R_V = 3.1 \pm 0.1$ , and width of the instability strip (WIS).

Filter	$\lambda_0^{\text{eff}}$ ( $\mu\text{m}$ )	$R_\lambda$	WIS (mag)
<i>BP</i>	0.5387	$3.106 \pm 0.102$	0.22
<i>V</i>	0.5525	$3.100 \pm 0.100$	0.22
<i>G</i>	0.6419	$2.446 \pm 0.080$	0.22
<i>RP</i>	0.7667	$1.826 \pm 0.060$	0.22
<i>I<sub>C</sub></i>	0.7980	$1.732 \pm 0.061$	0.14
<i>J</i>	1.2345	$0.753 \pm 0.027$	0.11
<i>H</i>	1.6393	$0.406 \pm 0.023$	0.09
<i>K</i>	2.1757	$0.242 \pm 0.015$	0.07
[3.6 $\mu\text{m}$ ]	3.545	$0.115 \pm 0.010$	0.07
[4.5 $\mu\text{m}$ ]	4.442	$0.081 \pm 0.010$	0.07
Wesenheit indices			
<i>W<sub>G</sub></i>	$G - 1.911 (BP - RP)$		0.10
<i>W<sub>VI</sub></i>	$I - 1.266 (V - I)$		0.08
<i>W<sub>JK</sub></i>	$K - 0.473 (J - K)$		0.07
<i>W<sub>VK</sub></i>	$K - 0.085 (V - K)$		0.08
<i>W<sub>H</sub></i>	$F160W - 0.386 (F555W - F814W)$		0.07

with an accuracy of a few hundredths of a magnitude across the sky needed for this study.

We make use of three different sources of reddening values for Milky Way Cepheids. The first one is the 3D dust maps by Green et al. (2019) based on homogeneous *Gaia*, Pan-STARRS 1 and 2MASS photometry. As a second method, we derive reddening values by comparing the observed color  $(V - I)_{\text{obs}}$  of Cepheids with their intrinsic color  $(V - I)_{\text{intr}}$  obtained from the period-color relation:  $(V - I)_{\text{intr}} = (0.25 \pm 0.01) \log P + (0.50 \pm 0.01)$  (Riess et al. 2022). Finally, we adopt as third estimate the reddening values from Trahin et al. (2021) obtained with the SPIPS algorithm (Mérand et al. 2015) for MW Cepheids having an optimal set of spectro-, photo- and interferometric data. In the Monte Carlo sampling procedure described in Sect. 3.3,  $E(B - V)$  values are selected randomly among these three catalogs for each star and the procedure is repeated over 10,000 iterations which is a method we use to account for the covariance of these methods. Finally, in the LMC and SMC we used the reddening maps by Skowron et al. (2021). Milky Way Cepheids are particularly affected by interstellar reddening: the stars of our MW sample have a mean  $E(B - V)$  of 0.5 mag (dispersion,  $\sigma = 0.3$  mag), while

in the LMC they have a mean  $E(B - V)$  of 0.11 mag ( $\sigma = 0.05$  mag) and of 0.05 mag ( $\sigma = 0.02$  mag) in the SMC. Reddening uncertainties are propagated through uncertainty in the reddening law in the next section.

### 2.3. Metallicity

For Milky Way Cepheids, we adopted in priority the iron abundances by Genovali et al. (2015) and complemented these values with the catalog by Genovali et al. (2014), with a mean uncertainty of 0.08 dex for both. The latter also provides additional abundances from the literature for 375 other Galactic Cepheids, for which we set the uncertainty to 0.1 dex. All metallicity measurements provided in these catalogs are rescaled to the same solar abundance. The weighted mean metallicity of our sample of Milky Way Cepheids is  $+0.085 \pm 0.022$  dex, with a dispersion of 0.123 dex. We adopt this mean value for the Galactic Cepheid sample in the following. Although Ripepi et al. (2021) published new abundances for a sample of 47 MW Cepheids, most of them either have an uncertain pulsation mode or do not have well sampled light curves in the selected filters of our study, therefore we were not able to use them. We note that additional constraining power is available by retaining the individual MW abundances in the analysis (Riess et al. 2021) but we have chosen the simpler host-to-host analysis for its transparency.

Romaniello et al. (2022) recently obtained high resolution spectra for 89 Cepheids in the LMC and derived their chemical abundances and revised the measurements of those from Romaniello et al. (2008). They concluded that they are consistent within the errors with a single common abundance of  $-0.409$  dex with a dispersion of 0.076 dex (similar to the uncertainty per measurement of 0.07 dex), which is more metal-poor by 0.1 dex and the breadth of the distribution is half as wide (see discussion in Romaniello et al. (2022)). We adopt this mean value for all LMC Cepheids with an uncertainty of 0.02 dex. In the SMC, we follow Gieren et al. (2018) and adopt a mean metal abundance of  $-0.75 \pm 0.05$  dex for all SMC Cepheids.

### 2.4. Distances

Distances to Milky Way Cepheids are taken from the Bailer-Jones et al. (2021) catalog based on the *Gaia* EDR3 parallaxes (Gaia Collaboration et al. 2021), as well as the associated uncertainties: we adopted the photogeometric distances which are derived using the  $(BP - RP)$  color,  $G$  magnitude, *Gaia* EDR3 parallaxes, and a direction-dependent prior accounting for the distribution of stellar distances along a line of sight and

for interstellar extinction. These distances include the Lindegren et al. (2021) zero-point correction on *Gaia* parallaxes. Lindegren et al. (2021) recommends to include an error of a few  $\mu\text{as}$  on the parallax zero-point so we assumed a  $5\ \mu\text{as}$  uncertainty, which is equivalent to including a systematic error of  $\sim 0.02\ \text{mag}$  in terms of distance modulus for this sample of MW Cepheids.

The Milky Way Cepheids are much brighter than most stars in the *Gaia* catalogue with visual magnitudes of 6-9 mag, brighter than the range where the *Gaia* zero-point is well-calibrated. As a result it is recommended by the *Gaia* team to derive the zero-point in this magnitude range independently from the luminosity using the PL relation. Following this procedure, Riess et al. (2021) found that the Lindegren et al. (2021) zero-point is overestimated by approximately  $14\ \mu\text{as}$ , which was confirmed by Zinn (2021) from asteroseismology of bright red giants. We therefore applied a small additional correction ( $dr$ ) to the Bailer-Jones et al. (2021) distances in order to take into account this zero-point. A good approximation of this correction is to take  $dr = -r^2 d\varpi$  where  $d\varpi = -0.014\ \text{mas}$  and  $r$  is the original Bailer-Jones et al. (2021) distance in kpc<sup>1</sup>. Finally, all Cepheids with a Renormalized Unit Weight Error (RUWE) parameter larger than 1.4 were excluded from the sample as likely astrometric binaries.

For LMC Cepheids, we adopt the most precise distance to this galaxy obtained by Pietrzyński et al. (2019) from a sample of 20 detached eclipsing binaries:  $49.59 \pm 0.09\ (\text{stat.}) \pm 0.54\ (\text{syst.})\ \text{kpc}$ . This corresponds to a full uncertainty of  $0.026\ \text{mag}$  in distance modulus. For more precision on the adopted distance, the position of each Cepheid in the LMC is taken into account by applying the planar geometry correction by Jacyszyn-Dobrzeńska et al. (2016) (see B21).

With the same technique and assumptions, Graczyk et al. (2020) published the most precise distance to the SMC from 15 eclipsing binary systems distributed around the core: they obtained a distance of  $62.44 \pm 0.47\ (\text{stat.}) \pm 0.81\ (\text{syst.})\ \text{kpc}$ . This is equivalent to a full uncertainty of  $0.032\ \text{mag}$  in distance modulus. To account for the elongated shape of the SMC along the line of sight, we include the geometric model fit to the DEBs and described by the blue lines in Figure 4 of Graczyk et al. (2020), their equations are provided

in B21 (we also limit the selection of SMC Cepheids to a separation of  $< 0.6\ \text{deg}$  between the Cepheids and the SMC center which together with the geometric correction we show greatly reduces their dispersion, see Sect. 3.1 and 5.4). Following Riess et al. (2019), we include these corrections directly on Cepheid magnitudes. Considering the standard deviation of three different geometry models, Riess et al. (2019) found a systematic uncertainty of  $0.002\ \text{mag}$  associated with the LMC geometry: we neglected this contribution to the error budget, since it is widely dominated by other systematics.

### 3. METHOD

#### 3.1. Sample selection

Among the Cepheid samples described in the previous section, a selection based on various criteria is performed. First, only fundamental mode Cepheids are considered: the pulsation modes are taken by order of priority from the Ripepi et al. (2019) reclassification, from Groenewegen (2018) and from the VSX database (Watson et al. 2006). A second selection is performed based on the number of epochs available for a given light curve. For the MW sample, only Cepheids with at least 8 data points are considered. Regarding the LMC and SMC samples, a large number of Cepheids have less than 8 measurements per light curve in the NIR and excluding them would drastically reduce the sample, therefore a limit of 5 epochs per star is adopted. For all Cepheids, a minimum uncertainty of 10% on mean magnitudes is adopted as a precision limit. Additionally, due to the non-negligible depth of the Magellanic Clouds (especially that of the SMC), Cepheids outside of a radius of  $3^\circ$  around the LMC center and  $0.6^\circ$  around the SMC center are excluded from the analysis. These regions are found to be optimal as they minimize the scatter of the PL relation (see Sect. 5.4) and together with the geometric correction reduces any potential separation from the mean of the DEBs. Finally, a selection based on pulsation periods is applied: due to a possible non-linearity of the PL relation at very short and very long periods or of overtones at short periods, the sample is limited to  $0.4 < \log P < 2$ .

#### 3.2. Width of the Instability Strip

The finite width of the instability introduces additional scatter in the PL relation and should be included quadratically as an uncertainty in apparent magnitudes. In Riess et al. (2019), the width of the instability strip is obtained by taking the scatter of the PL relation

<sup>1</sup> The best way to include the additional  $0.014\ \text{mas}$  offset would be to infer new corrected distances using the Bailer-Jones et al. (2021) method, however it would be beyond the scope of this paper and would give similar results in terms of precision. A comparison for a few sources shows that the approximate approach is reliable to account for this correction (C. A. L. Bailer-Jones, private communication).

(0.075 mag from their Table 3), and by subtracting quadratically the errors on photometric measurements (e.g. photometric inhomogeneities, phase corrections) which are of 0.030 mag. They obtained an intrinsic width of 0.069 mag for the instability strip in the  $W_H$  index. Similarly, the values in the  $V$  and  $I$  bands are 0.22 mag and 0.14 mag (Macri et al. 2006). In the  $J$ ,  $H$  and  $K$  bands, the study by Persson et al. (2004) gives a width of 0.11 mag, 0.09 mag and 0.07 mag for the NIR instability strip. For *Spitzer* bands, we adopted a width of 0.07 mag (Scowcroft et al. 2011; Monson et al. 2012). Finally, it is difficult to estimate the width of the instability strip in *Gaia* bands because most calibrations from the literature either use Wesenheit indices or provide PL relations without correcting the extinction. Assuming that the  $G$ ,  $BP$  and  $RP$  bands are similar to the  $V$  band in terms of wavelength and PL dispersion, the width of the instability strip in *Gaia* bands is set to 0.22 mag. These values are listed in Table 3.

### 3.3. Period-luminosity-metallicity relation

The absolute magnitude  $M_\lambda$  of a star is derived from its apparent magnitude  $m_\lambda$ , its reddening  $E(B-V)$  and its distance  $d$  in kpc by the equation:

$$M_\lambda = m_\lambda - R_\lambda E(B-V) - 5 \log d - 10 \quad (2)$$

Apparent magnitudes are corrected for the extinction using the Wang & Chen (2019) reddening law with parameter  $R_V = 3.1 \pm 0.1$  which yields the  $R_\lambda$  values listed in Table 3. The uncertainty of 0.1 in  $R_V$  and its propagation to other filters is intended to characterize the line-of-sight dispersion seen for similar stellar populations. Five Wesenheit indices are also considered (Madore 1982), based on a combination of optical and NIR filters, such that  $W(\lambda_1, \lambda_2, \lambda_3) = m_{\lambda_1} - R(m_{\lambda_2} - m_{\lambda_3})$  with  $R = R_{\lambda_1}/(R_{\lambda_2} - R_{\lambda_3})$ . For the HST Wesenheit  $W_H$  we adopt  $R = 0.386 \pm 0.02$  (Riess et al. 2022).

To measure the metallicity effect  $\gamma$  between the Galactic, LMC and SMC samples, the PL relation of the form

$$M = \alpha (\log P - \log P_0) + \beta \quad (3)$$

is first fitted in each of the three galaxies, with a common slope  $\alpha$  fixed to that of the LMC (since it has the largest number of Cepheids, the lowest PL dispersion and the slope least affected by non-uniformity of individual Cepheid distances). The three PL intercepts  $\beta$  are obtained from Monte Carlo sampling of the data and error distributions with 10,000 iterations: to ensure the robustness of the fit, the apparent magnitudes, distances,  $R_V$  and  $E(B-V)$  values are free to vary within the uncertainties during each iteration. In the case of the MW

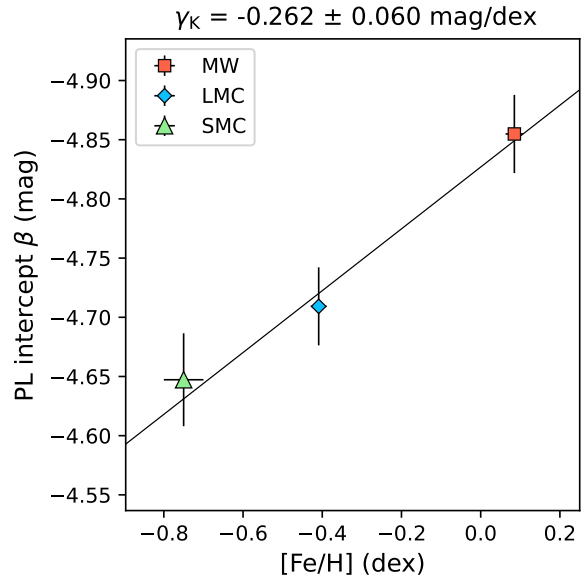


**Figure 1.** PL intercept ( $\beta$ ) in the  $K$  band fitted with a common slope in the Milky Way, LMC and SMC as a function of the mean metallicity ( $[\text{Fe}/\text{H}]$ ) of the galaxy (Eq. 4).

sample, the  $E(B-V)$  values are selected randomly for each star among the three previously described measures of extinction (see Table 2) which will naturally account for their covariance. Systematic uncertainties due to photometric zero-points (see Sect. 2.1) and to distance measurements (see Sect. 2.4) are included quadratically to the intercept errors in the three galaxies. Finally, the metallicity term  $\gamma$  of the PL relation as defined in Eq. 1 is obtained by fitting (again with Monte Carlo sampling) the relation:

$$\beta = \gamma [\text{Fe}/\text{H}] + \delta \quad (4)$$

where  $\beta$  is the intercept of the PL relation,  $[\text{Fe}/\text{H}]$  is the mean metallicity in each of the three galaxies and  $\delta$  is the fiducial luminosity at  $\log P = 0.7$  and solar metallicity. As an example, Fig. 1 illustrates the linear fit of Eq. 4 in the  $K$  band.

## 4. RESULTS

### 4.1. The PL relation

In Sect. 4.2, the metallicity term ( $\gamma$ ) of the PL relation is derived when the slopes ( $\alpha$ ) are fixed to the same value in the three galaxies, in order to directly compare the intercepts ( $\beta$ ). However in this section we first calibrated the PL relation of the form  $M = \alpha(\log P - 0.7) + \beta$  in each galaxy where both the slope and the intercept are free to vary. This allows to check the consistency of the slopes in the three galaxies of different chemical composition. The coefficients are listed in Table 4 and

**Table 4.** Results of the PL fit of the form  $M = \alpha(\log P - 0.7) + \beta$  in the Milky Way, LMC and SMC. In column 3 and 4,  $\alpha_{\text{free}}$  and  $\beta_{\text{free}}$  are obtained when both coefficients are free parameters. In columns 5 and 6,  $\beta$  is the intercept obtained with the slope  $\alpha_{\text{fixed}}$  fixed to that of the LMC.

Filter	Galaxy	$\alpha_{\text{free}}$	$\beta_{\text{free}}$	$\alpha_{\text{fixed}}$	$\beta$	$\sigma$	$N_{\text{stars}}$
<i>BP</i>	MW	$-2.767 \pm 0.163$	$-3.084 \pm 0.063$	$-2.636 \pm 0.044$	$-3.108 \pm 0.066$	0.36	156
	LMC	$-2.636 \pm 0.044$	$-3.013 \pm 0.031$	$-2.636 \pm 0.044$	$-3.013 \pm 0.031$	0.22	492
	SMC	$-2.357 \pm 0.077$	$-2.950 \pm 0.037$	$-2.636 \pm 0.044$	$-2.946 \pm 0.038$	0.28	229
<i>V</i>	MW	$-2.775 \pm 0.140$	$-3.331 \pm 0.069$	$-2.728 \pm 0.038$	$-3.343 \pm 0.068$	0.34	184
	LMC	$-2.728 \pm 0.038$	$-3.181 \pm 0.036$	$-2.728 \pm 0.038$	$-3.182 \pm 0.036$	0.19	714
	SMC	$-2.578 \pm 0.073$	$-3.082 \pm 0.042$	$-2.728 \pm 0.038$	$-3.083 \pm 0.042$	0.27	284
<i>G</i>	MW	$-2.856 \pm 0.117$	$-3.468 \pm 0.057$	$-2.847 \pm 0.039$	$-3.469 \pm 0.054$	0.33	166
	LMC	$-2.847 \pm 0.039$	$-3.273 \pm 0.029$	$-2.847 \pm 0.039$	$-3.274 \pm 0.029$	0.17	617
	SMC	$-2.695 \pm 0.066$	$-3.184 \pm 0.037$	$-2.847 \pm 0.039$	$-3.181 \pm 0.036$	0.24	251
<i>RP</i>	MW	$-2.887 \pm 0.106$	$-3.924 \pm 0.045$	$-2.907 \pm 0.039$	$-3.921 \pm 0.044$	0.29	147
	LMC	$-2.907 \pm 0.039$	$-3.806 \pm 0.029$	$-2.907 \pm 0.039$	$-3.807 \pm 0.029$	0.15	492
	SMC	$-2.760 \pm 0.064$	$-3.720 \pm 0.036$	$-2.907 \pm 0.039$	$-3.716 \pm 0.036$	0.21	229
<i>I</i>	MW	$-2.958 \pm 0.109$	$-3.932 \pm 0.049$	$-2.960 \pm 0.023$	$-3.933 \pm 0.047$	0.26	157
	LMC	$-2.960 \pm 0.023$	$-3.844 \pm 0.034$	$-2.960 \pm 0.023$	$-3.844 \pm 0.034$	0.14	743
	SMC	$-2.966 \pm 0.036$	$-3.774 \pm 0.039$	$-2.960 \pm 0.023$	$-3.774 \pm 0.039$	0.21	298
<i>J</i>	MW	$-3.100 \pm 0.081$	$-4.492 \pm 0.040$	$-3.155 \pm 0.015$	$-4.481 \pm 0.038$	0.19	68
	LMC	$-3.155 \pm 0.015$	$-4.337 \pm 0.038$	$-3.155 \pm 0.015$	$-4.337 \pm 0.038$	0.11	775
	SMC	$-2.974 \pm 0.035$	$-4.255 \pm 0.040$	$-3.155 \pm 0.015$	$-4.251 \pm 0.040$	0.17	263
<i>H</i>	MW	$-3.166 \pm 0.071$	$-4.743 \pm 0.036$	$-3.176 \pm 0.012$	$-4.741 \pm 0.035$	0.18	68
	LMC	$-3.176 \pm 0.012$	$-4.668 \pm 0.037$	$-3.176 \pm 0.012$	$-4.668 \pm 0.037$	0.09	771
	SMC	$-3.183 \pm 0.021$	$-4.574 \pm 0.039$	$-3.176 \pm 0.012$	$-4.573 \pm 0.039$	0.17	287
<i>K</i>	MW	$-3.194 \pm 0.061$	$-4.865 \pm 0.035$	$-3.237 \pm 0.010$	$-4.855 \pm 0.033$	0.17	64
	LMC	$-3.237 \pm 0.010$	$-4.709 \pm 0.033$	$-3.237 \pm 0.010$	$-4.709 \pm 0.033$	0.08	774
	SMC	$-3.184 \pm 0.016$	$-4.648 \pm 0.039$	$-3.237 \pm 0.010$	$-4.647 \pm 0.039$	0.15	297
[3.6 $\mu\text{m}$ ]	MW	$-3.551 \pm 0.072$	$-4.812 \pm 0.041$	$-3.339 \pm 0.050$	$-4.891 \pm 0.031$	0.15	20
	LMC	$-3.339 \pm 0.050$	$-4.779 \pm 0.033$	$-3.339 \pm 0.050$	$-4.779 \pm 0.027$	0.10	82
	SMC	$-3.616 \pm 0.063$	$-4.536 \pm 0.049$	$-3.339 \pm 0.050$	$-4.690 \pm 0.035$	0.10	23
[4.5 $\mu\text{m}$ ]	MW	$-3.474 \pm 0.080$	$-4.806 \pm 0.041$	$-3.247 \pm 0.050$	$-4.889 \pm 0.031$	0.16	20
	LMC	$-3.247 \pm 0.050$	$-4.810 \pm 0.032$	$-3.247 \pm 0.050$	$-4.810 \pm 0.027$	0.11	82
	SMC	$-3.580 \pm 0.063$	$-4.571 \pm 0.050$	$-3.247 \pm 0.050$	$-4.758 \pm 0.035$	0.11	23
<i>W<sub>G</sub></i>	MW	$-3.256 \pm 0.046$	$-5.057 \pm 0.024$	$-3.387 \pm 0.018$	$-5.037 \pm 0.023$	0.21	146
	LMC	$-3.387 \pm 0.018$	$-4.805 \pm 0.026$	$-3.387 \pm 0.018$	$-4.805 \pm 0.026$	0.10	493
	SMC	$-3.404 \pm 0.025$	$-4.678 \pm 0.033$	$-3.387 \pm 0.018$	$-4.679 \pm 0.033$	0.16	227
<i>W<sub>VI</sub></i>	MW	$-3.124 \pm 0.036$	$-4.768 \pm 0.039$	$-3.280 \pm 0.013$	$-4.738 \pm 0.039$	0.19	156
	LMC	$-3.280 \pm 0.013$	$-4.680 \pm 0.039$	$-3.280 \pm 0.013$	$-4.680 \pm 0.039$	0.08	712
	SMC	$-3.254 \pm 0.021$	$-4.634 \pm 0.043$	$-3.280 \pm 0.013$	$-4.634 \pm 0.043$	0.14	284
<i>W<sub>JK</sub></i>	MW	$-3.211 \pm 0.059$	$-5.031 \pm 0.039$	$-3.281 \pm 0.011$	$-5.015 \pm 0.037$	0.16	62
	LMC	$-3.281 \pm 0.011$	$-4.887 \pm 0.043$	$-3.281 \pm 0.011$	$-4.886 \pm 0.043$	0.08	775
	SMC	$-3.286 \pm 0.016$	$-4.822 \pm 0.045$	$-3.281 \pm 0.011$	$-4.822 \pm 0.045$	0.14	264
<i>W<sub>VK</sub></i>	MW	$-3.156 \pm 0.070$	$-5.014 \pm 0.042$	$-3.262 \pm 0.012$	$-4.989 \pm 0.039$	0.17	55
	LMC	$-3.262 \pm 0.012$	$-4.837 \pm 0.039$	$-3.262 \pm 0.012$	$-4.837 \pm 0.039$	0.07	720
	SMC	$-3.230 \pm 0.019$	$-4.779 \pm 0.044$	$-3.262 \pm 0.012$	$-4.779 \pm 0.044$	0.15	283
<i>W<sub>H</sub></i>	MW	$-3.363 \pm 0.054$	$-4.950 \pm 0.027$	$-3.305 \pm 0.039$	$-4.965 \pm 0.024$	0.17	61
	LMC	$-3.305 \pm 0.039$	$-4.822 \pm 0.032$	$-3.305 \pm 0.039$	$-4.821 \pm 0.028$	0.08	69
	SMC	–	–	–	–	–	–

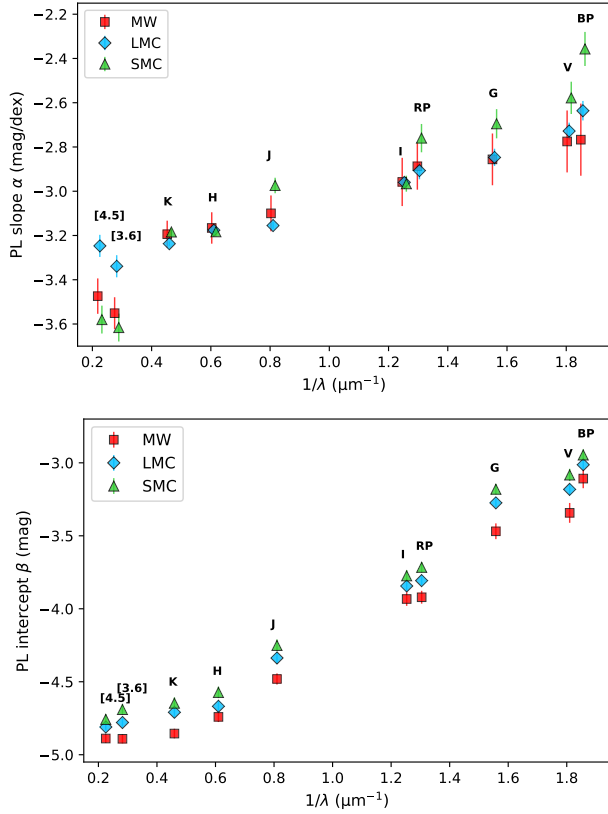


**Figure 2. Top:** PL slope ( $\alpha$ ) in the Milky Way and Magellanic Clouds represented with wavelength. **Bottom:** PL intercept ( $\beta$ ) obtained in the Milky Way and Magellanic Clouds with a slope fixed to that of the LMC, represented with wavelength.

represented in Fig. 2. In all filters, the PL slope obtained for the LMC sample is in agreement to better than  $3\sigma$  with that in the MW and SMC samples, except for the  $J$  band and  $[4.5\ \mu\text{m}]$  band where the LMC and SMC slopes differ by  $4\sigma$ . Overall, we see no strong evidence to reject the hypothesis of a common slope in the three galaxies (see Sect. 4.2).

As expected, the dispersion of the PL relation decreases significantly from the optical to the infrared, which is directly a consequence of the sensitivity of each filter to the extinction and of the width of the instability strip. In the Milky Way as well as in both Magellanic Clouds, the PL slope  $\alpha$  becomes steeper and the PL intercept  $\beta$  becomes more negative (i.e. brighter) from the optical towards the infrared. Only the *Spitzer*  $[4.5\ \mu\text{m}]$  band does not follow this trend, which was already noticed by Marengo et al. (2010), Freedman et al. (2011) and Scowcroft et al. (2011). This may be due to the presence of a large CO absorption band aligned with the  $[4.5\ \mu\text{m}]$  filter. For this reason, in section 5.3, the  $[4.5\ \mu\text{m}]$  filter is ignored in the fit of the  $\gamma = f(\lambda)$  re-

lation. In the Wesenheit  $W_H$  band we obtain a slope of  $-3.305 \pm 0.039$  mag/dex in the LMC which is fully compatible with the slope of  $-3.299 \pm 0.015$  mag/dex derived by the SH0ES team (Riess et al. 2022).

In the Milky Way, the PL relation generally shows a larger dispersion than in the Magellanic Clouds because of the higher extinction and non-uniform distances. The PL relations in Wesenheit indices show a low dispersion, as expected from their insensitivity to extinction. In some filters only a small number of Cepheids is listed in Table 4: this is due to the various selection criteria applied to the samples, such as the upper limit of 1.4 on the RUWE parameter, the limited radius around the SMC center and the cuts in periods. Finally, for a given filter, the PL intercept in the Milky Way is more negative than in the LMC and even more than in the SMC, indicating a negative sign for the  $\gamma$  term.

#### 4.2. The PLZ relation

After fixing the slope of the PL relation to that of the LMC (Table 4) in the three galaxies, we solve for Eq. 4 with a Monte Carlo sampling where both the intercepts ( $\beta$ ) and the mean  $[\text{Fe}/\text{H}]$  values of each sample are free to vary within their error bars. The  $\gamma$  and  $\delta$  coefficients obtained for the PLZ relation are listed in Table 5.

All  $\gamma$  values over a wavelength range of  $0.5 - 4.5\ \mu\text{m}$  are negative (with a significance of  $1.8\sigma$  to  $8.5\sigma$ ), meaning that metal-rich Cepheids are brighter than metal-poor ones. The  $\gamma$  values range between  $-0.122 \pm 0.069$  mag/dex (in  $W_{VI}$ ) and  $-0.444 \pm 0.052$  mag/dex (in  $W_G$ ) with a dispersion of  $0.06$  mag/dex. In all filters, the  $\gamma$  values are in good agreement with those obtained by Gieren et al. (2018) and B21, especially in the NIR, but significantly stronger than the effect detected by Wielgórski et al. (2017), which was close to zero (see discussion in Sect. 5.4). The metallicity effect in *Gaia* filters is similar to that in ground optical filters ( $V$ ,  $I$ ), however the  $G$  band and  $W_G$  Wesenheit index show a stronger effect (see discussion in Sect. 5.1).

We note that our  $\gamma$  value in  $W_{VI}$  is slightly weaker than other estimates from the literature, although they are consistent within the error bars. While the optical photometry for LMC and SMC Cepheids is in the same system (OGLE-IV) and their comparison produces a stronger  $\gamma$  term, apparent  $V$  and  $I$  magnitudes for Galactic Cepheids are taken from Berdnikov (2008), a compilation of disparate observations made with various instruments, and a larger-than-budgeted zeropoint difference may explain this difference. Additionally, using HST photometry in  $F555W$  and  $F814W$  (Riess et al. 2019, 2021) in place of  $V$  and  $I$  respectively returns a

**Table 5.** Results of the fit of the form  $\beta = \gamma [\text{Fe}/\text{H}] + \delta$  (Eq. 4) obtained from a comparison of the PL intercepts ( $\beta$ ) in the Milky Way, LMC and SMC. The slope  $\alpha$  is fixed to that of the LMC sample (see Table 4).

Filter	$\gamma$	$\sigma$	$\delta$	$\sigma$	$N_{\text{stars}}$
<i>BP</i>	-0.195	0.091	-3.092	0.047	877
<i>V</i>	-0.312	0.098	-3.312	0.050	1182
<i>G</i>	-0.350	0.081	-3.427	0.041	1034
<i>RP</i>	-0.241	0.069	-3.903	0.034	868
<i>I</i>	-0.189	0.076	-3.919	0.037	1198
<i>J</i>	-0.278	0.067	-4.455	0.032	1106
<i>H</i>	-0.184	0.064	-4.730	0.029	1126
<i>K</i>	-0.262	0.060	-4.828	0.026	1135
[3.6 $\mu\text{m}$ ]	-0.236	0.059	-4.872	0.026	125
[4.5 $\mu\text{m}$ ]	-0.158	0.057	-4.875	0.025	125
<i>W<sub>G</sub></i>	-0.444	0.052	-4.996	0.021	866
<i>W<sub>VI</sub></i>	-0.122	0.069	-4.729	0.032	1152
<i>W<sub>JK</sub></i>	-0.239	0.069	-4.992	0.032	1101
<i>W<sub>VK</sub></i>	-0.267	0.072	-4.960	0.033	1058
<i>W<sub>H</sub></i> (*)	-0.291	0.075	-4.940	0.021	130

**Note:** (\*) Does not include SMC sample (no HST photometry) or individual metallicities in the MW or Cepheids in SN Ia hosts as used in [Riess et al. \(2022\)](#).

steeper metallicity effect of about  $-0.2 \text{ mag/dex}$ , closer to the value from the literature (although it does not include the SMC sample for which there is no HST photometry available).

Finally, in the  $W_H$  Wesenheit index based on pure HST photometry of Milky Way and LMC Cepheids, we obtain a metallicity effect of  $-0.291 \pm 0.075 \text{ mag/dex}$ , in agreement with the value of  $-0.217 \pm 0.046 \text{ mag/dex}$  derived by the SH0ES team from a broader range of data from the MW, LMC, SMC, NGC 4258 and gradients in SN Ia hosts ([Riess et al. 2022](#)).

We tested the hypothesis of a common slope in the three galaxies by fixing the slope to that of the SMC sample instead of that of the LMC one: we obtained similar  $\gamma$  values at the  $0.4\sigma$  level or better, confirming the validity of our hypothesis.

## 5. DISCUSSION

### 5.1. Potential issues with the *Gaia G* filter

In the *Gaia* Wesenheit index  $W_G$ , we derive a strong effect of  $-0.444 \pm 0.052 \text{ mag/dex}$ , confirming the previous result by [Ripepi et al. \(2022\)](#) who obtained  $-0.520 \pm 0.090 \text{ mag/dex}$  from Milky Way Cepheids. The metallicity effect in this Wesenheit index is surprisingly strong compared to other filters or other Wesenheit

indices, but is comparable to that in the *Gaia G* band. This could be explained by the particularly large width of the *G* filter (almost 800 nm) and suggests that the results based on *Gaia G* band photometry should be treated particularly carefully. For these reasons, the *G* band is ignored in the fit of the relation between  $\gamma$  and  $\lambda$  in Fig. 3. Additionally, Wesenheit indices have been established to minimize the effects of interstellar extinction, however they are not totally independent of the reddening law since they rely on the *R* coefficient (see Sect. 3).

### 5.2. Reddening law

The correction for dust extinction and the assumption of a reddening law are critical steps in the calibration of the distance scale. The parameter  $R_V = A_V/E(B - V)$  is related to the average size of dust grains and gives a physical basis for the variations in extinction curves. Although the differences in  $R_V$  are relatively small between the Milky Way and Magellanic Clouds, they can still impact the calibration of the Leavitt law. In the Milky Way, most studies are based on the assumption  $R_V = 3.1$  ([Cardelli et al. 1989](#)), while [Gordon et al. \(2003\)](#) report an average of  $R_V = 3.41 \pm 0.06$  in the LMC and  $R_V = 2.74 \pm 0.13$  in the SMC. They conclude that LMC and SMC extinction curves are similar qualitatively to those derived in the Milky Way. But even in the Milky Way the extinction curve was shown to be highly spatially variable ([Fitzpatrick et al. 2019](#)).

Assuming a different reddening law or  $R_V$  value across different galaxies is possible but more complex (see [Riess et al. 2022](#), Appendix D). Since the *R* ratio in Wesenheit indices multiplies a color term, it requires to separate the contribution of the color that results from dust reddening by first subtracting the intrinsic color of Cepheids, which can be done using a period-color relation. However, [Riess et al. \(2022\)](#) concluded that determining individual values of *R* was not very informative due to large uncertainties on both color and brightness.

In the present work, we assumed a uniform  $R_V$  value of 3.1 but we include an uncertainty of 0.1 on this parameter, which is usually neglected in most studies, even when combining Cepheid samples in different galaxies. For each  $R_\lambda$  value, we also included the uncertainties on the  $A_\lambda/A_V$  ratios listed in [Wang & Chen \(2019\)](#).

### 5.3. A relationship between $\gamma$ and $\lambda$

As the filters used in this analysis cover a large wavelength range, we can measure a dependence between the metallicity term  $\gamma$  and the wavelength. When fitting a

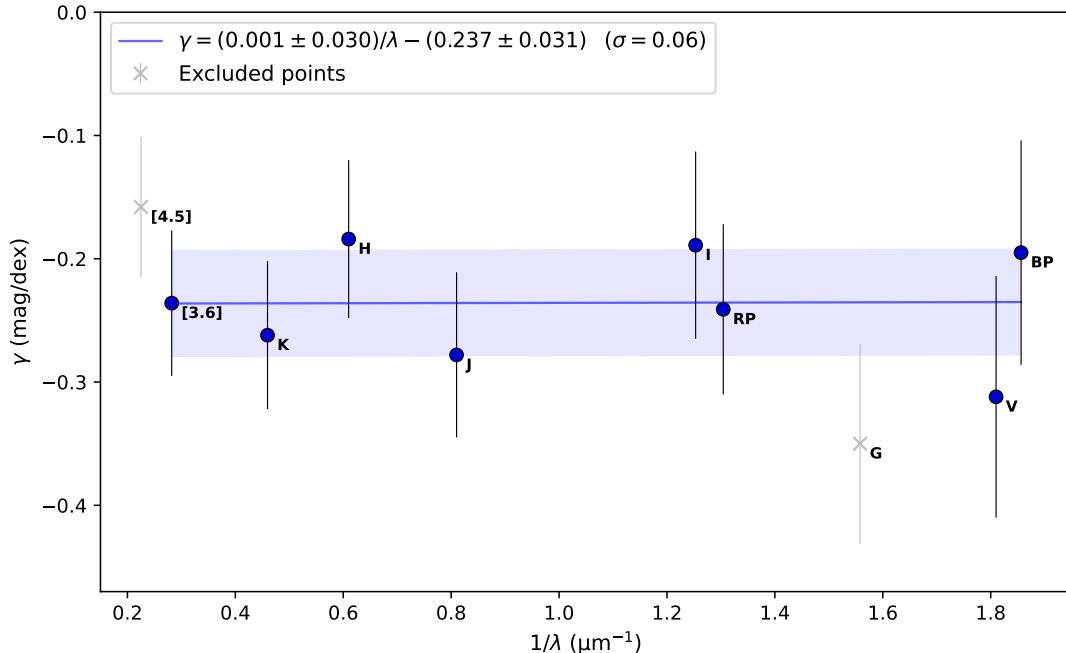


**Figure 3.** Metallicity effect ( $\gamma$ ) as a function of wavelength ( $\lambda$ ).

linear relationship between  $\gamma$  and  $1/\lambda$  through the points of Fig. 3 after excluding the  $[4.5 \mu\text{m}]$  filter (see Sect. 4.1) and the  $G$  band (see Sect. 5.1), we derive the following relation:

$$\gamma = \frac{0.001 \pm 0.030}{\lambda} - (0.237 \pm 0.031) \quad (5)$$

with  $\sigma = 0.06$  mag/dex. The slope of Eq. 5 shows that the metallicity effect is uniform over the wavelength range  $0.5 - 4.5 \mu\text{m}$ . Compared to the luminosity dependence it suggests that Cepheid colors are relatively insensitive to metallicity. To verify this is not related to any use of Cepheid colors to estimate reddening, when the reddening estimates based on color are discarded from the analysis (i.e. only the reddening maps by Green et al. (2019) are used), we obtain a similar flat slope ( $-0.003 \pm 0.031$  mag/dex) which confirms the previous finding.

#### 5.4. Comparison with other empirical estimates of $\gamma$

The recognition of a  $\gamma$  term is relatively recent owing to necessary improvements in data quality (i.e., parallaxes, reddenings, Cepheid photometry, metallicity and Cloud geometry) which have accrued in the last two decades. In this section, we aim at identifying sources of differences with some previous studies. We represent some of these previously published values of the metallicity effect in Fig. 4.

Freedman & Madore (2011) used spectroscopic  $[\text{Fe}/\text{H}]$  abundances of 22 individual LMC Cepheids whose

metallicities were measured by Romaniello et al. (2008), covering a range of about 0.6 dex. They derived a negative metallicity effect in the mid-IR, cancelling in the NIR and becoming positive in optical wavelengths. However, Romaniello et al. (2022) published new abundances for a larger sample of LMC Cepheids and report this time a very narrow distribution of metallicities ( $\sigma = 0.1$  dex including systematics). They also note that the abundances provided in Romaniello et al. (2008) were significantly affected by a systematic error in the data reduction and analysis, and they confirm that the previous data are compatible with the same narrow spread observed for the new values. This shows that the LMC cannot be used to internally measure the metallicity effect and explains differences in the findings of Freedman & Madore (2011) (see Romaniello et al. 2022, for further discussion).

Wielgórski et al. (2017) performed a purely differential calibration of the  $\gamma$  term by comparing the Leavitt law across the full span of the LMC and SMC. Assuming the detached eclipsing binary distance by Pietrzyński et al. (2013) and Graczyk et al. (2014) respectively, they obtained a metallicity effect consistent with zero in the optical and NIR. Updating the mean LMC metallicity with the recent value by Romaniello et al. (2022) or/and replacing the DEB distances by the most precise ones by Pietrzyński et al. (2019) and Graczyk et al. (2020) does not yield significant differences with the Wielgórski et al. (2017) results. However, we find that the size of the re-

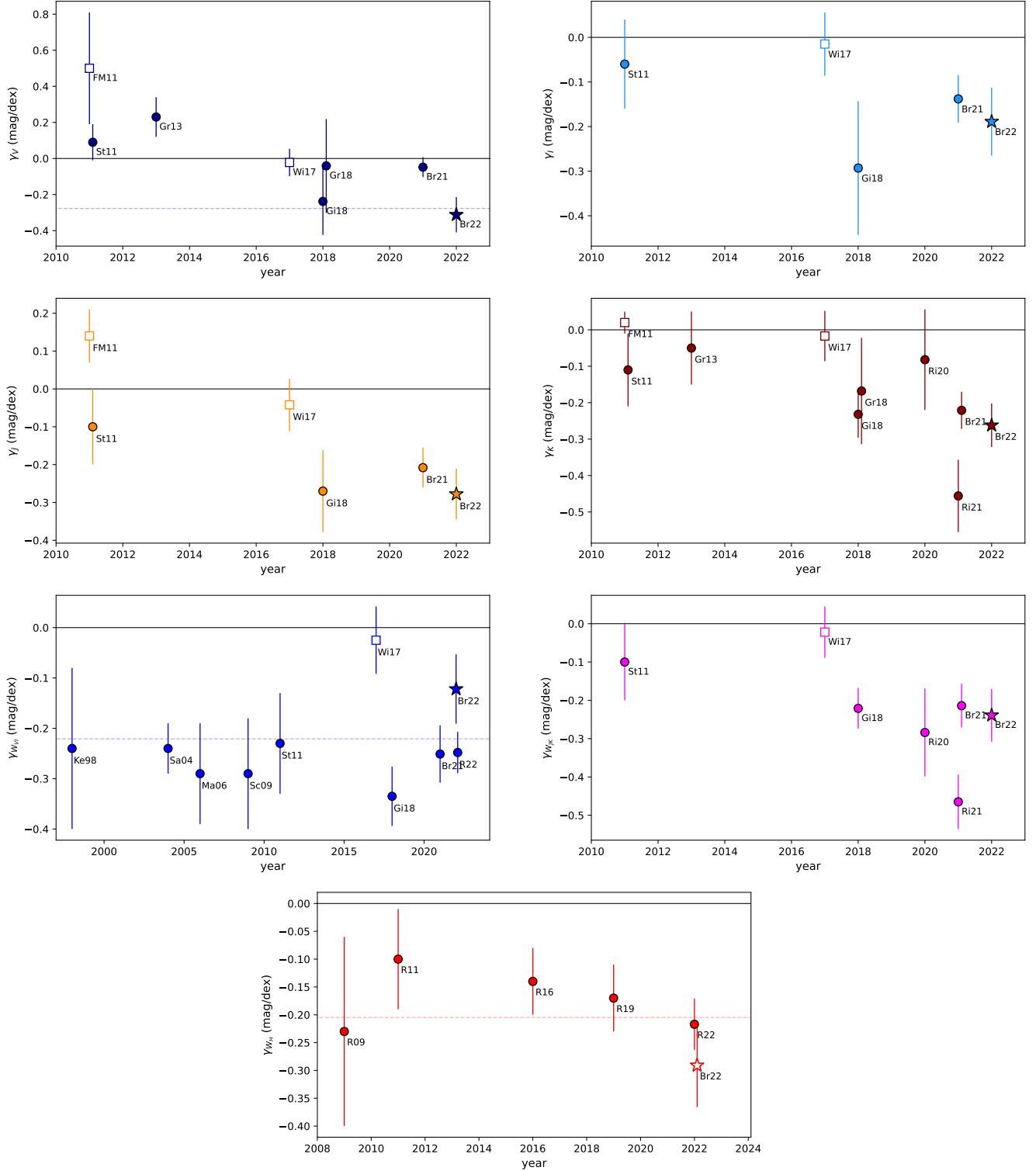


**Figure 4.** Evolution of the metallicity term  $\gamma$  in different filters over time. Open square symbols indicate the studies in which we identified issues which likely affect the accuracy of the corresponding  $\gamma$  values. The open star symbol in the bottom figure indicates that the present work in  $W_H$  does not include HST photometry for the SMC sample. **References:** (Ke98): Kennicutt et al. (1998), (Sa04): Sakai et al. (2004), (Ma06): Macri et al. (2006), (Sc09): Scowcroft et al. (2009), (R09): Riess et al. (2009), (FM11): Freedman & Madore (2011), (St11): Storm et al. (2011a), (R11): Riess et al. (2011), (Gr13): Groenewegen (2013), (R16): Riess et al. (2016), (Wi17): Wielgórski et al. (2017), (Gi18): Gieren et al. (2018), (Gr18): Groenewegen (2018), (R19): Riess et al. (2019), (Ri20): Ripepi et al. (2020), (Ri21): Ripepi et al. (2021), (R22): Riess et al. (2022), (Br21): Breuval et al. (2021), (Br22): present work. The dashed colored line represents the prediction of  $\gamma$  from Anderson et al. (2016) using Geneva evolution models including the effects of rotation.

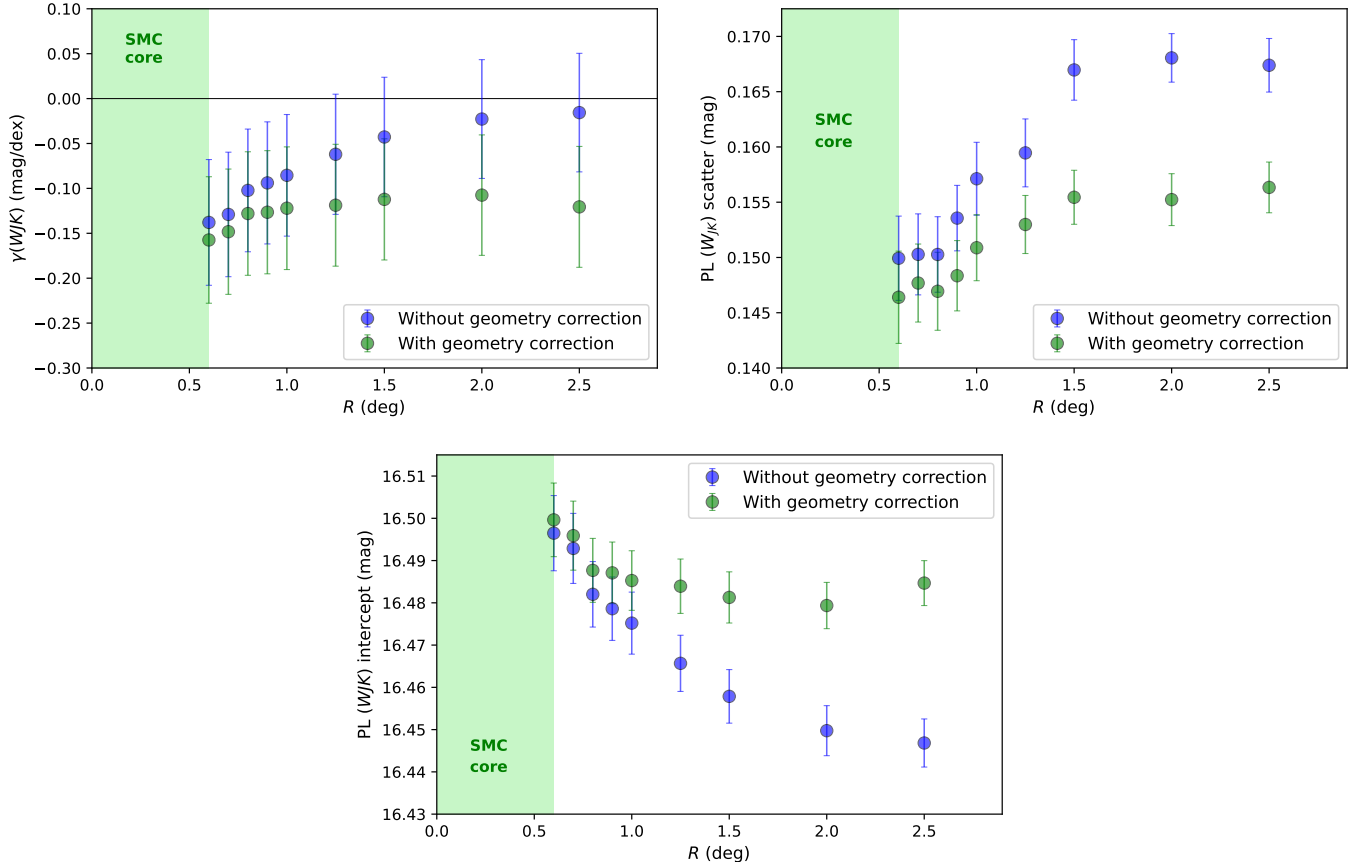


**Figure 5.** Metallicity effect ( $\gamma$ ) (top left panel), PL scatter (top right panel) and PL intercept (bottom panel) in the  $W_{JK}$  band as a function of the radius of the SMC region considered. The values are based on the dataset and method adopted by Wielgórski et al. (2017). Blue points are the values found in the same conditions as Wielgórski et al. (2017) and green points represent the values obtained after correcting for the SMC geometry (Graczyk et al. 2020).

gion and its depth considered around the SMC center considerably impacts the value of the  $\gamma$  term. The sensitivity of  $\gamma$  to the size of the region adopted in the SMC is due to the elongated shape of this galaxy along the line of sight. Despite the geometry correction performed in Sect. 2.4, Cepheids at larger distance to the SMC center show a larger scatter, as shown in Fig. 5, likely due to the shortcoming of the planar model at greater radii (and farther from the region it was defined by the DEBs). Thus the distances to Cepheids in outer regions of the SMC may differ significantly from the mean SMC distance modeled from the DEBs, perhaps due to the structures of the Magellanic stream (Nidever et al. 2008).

We can reproduce the findings of Wielgórski et al. (2017) by neglecting the correction for the SMC geometry and when considering all SMC Cepheids ( $R > 2$  deg) for which we obtain the same low metallicity dependence as Wielgórski et al. (2017). However the  $\gamma$  term becomes more negative when we retain Cepheids in a smaller region and it reaches  $-0.150$  mag/dex for  $R < 0.6$  deg.

When the geometry of the SMC is included in apparent magnitudes,  $\gamma$  is particularly stable between  $R = 0.6$  deg and  $R = 2$  deg with a value of  $-0.150$  mag/dex. This demonstrates that the very low metallicity effect found by Wielgórski et al. (2017) is likely due to unaccounted for differences in depth: limiting their analysis to a narrower region of the SMC and applying geometry corrections would yield a  $\gamma$  value no longer consistent with zero. We note that the  $\gamma$  values described in this section and represented in Fig. 5 differ from our results listed in Table 5 since they are based on the data and method from Wielgórski et al. (2017) (i.e. LMC and SMC samples only).

Owens et al. (2022) (hereafter OW22) compared Cepheids and geometric distances in the MW, LMC, and SMC and claim poor agreement, attributing this to an error in Gaia EDR3 parallaxes and proposing a large, positive Gaia parallax offset coupled with no Cepheid metallicity term (including for the commonly found one in  $W_{VI}$ ), with the consequence of a shorter Cepheid dis-

tance scale and higher Hubble constant<sup>2</sup>. There are numerous, important differences in the data used by OW22 and ours. OW22 largely employs older and less consistently calibrated photometry and reddening estimates<sup>3</sup> and a much smaller sample of MW Cepheids in the optical, 37 vs the  $\sim 150$  used here. We also use specific high-quality, space-based Cepheid photometry from HST (MW, LMC) and Gaia (MW, LMC, SMC) not used in the OW22 study. It is beyond the scope of this study to analyze the impacts of the older and newer data samples but we would not be surprised if they produce systematic differences at the few hundredths of a magnitude level relevant to the  $\sim 0.1$  mag effects of metallicity (e.g., between the LMC and SMC).

However, we identify two specific differences in the measurements between the LMC and SMC which appear to impact the OW22 calculation and which are independent of Gaia and its calibration. The difference in distance between the DEBs in the LMC and SMC is given by Graczyk et al. (2020) as  $0.500 \pm 0.017$  mag. The excess difference we find between the SMC core and the LMC (Table 4) averaged across all bands is 0.08 mag (SMC Cepheids are net fainter). For the 0.34 dex difference in Cloud metallicity, the metallicity term is then  $\sim 0.24$  mag per dex. OW22 give a best differential distance of  $0.511 \pm 0.056$  mag, for an excess of 0.01 mag, 0.07 mag smaller than found here and implying a negligible metallicity term in all bands (including the Wesenheit band,  $W_{VI}$  which has generally been found

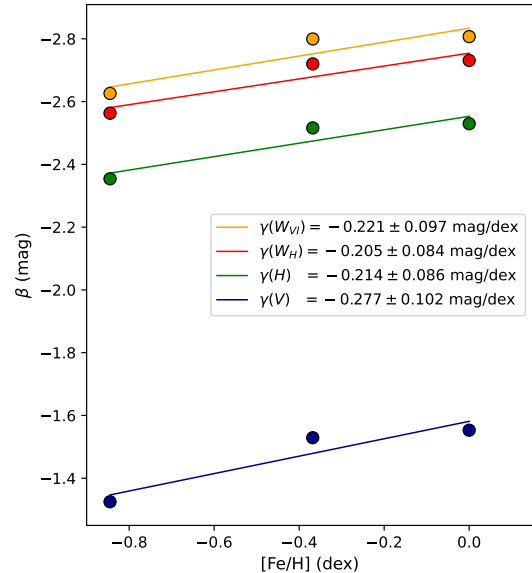


**Figure 6.** Metallicity effect predicted by Anderson et al. (2016) using the Geneva evolution models including rotation.

to be  $-0.2$  mag/dex, see Table 1). However, as Figure 5 shows the depth of the SMC at large radii adds dispersion and reduces the apparent distance. The OW22 study uses SMC data from Scowcroft et al. (2016) with a radius from the core of up to 2 degrees. Scowcroft et al. (2016) also noted a large spatial dependence in Cepheid distance across the greater region of the SMC. The combination of correcting for the geometry (of 0.03 mag, given but not applied in OW22) and limiting to the core ( $< 0.6$  degrees here) accounts for 0.06 mag of the 0.07 mag difference with our study and thus the difference between a moderate or negligible metallicity term in all bands. We think the known depth of the SMC and observed reduction in Cepheid PL scatter by correcting for the DEB-based geometry and limiting to the core where most of the DEBs are found provides a strong argument this yields a more accurate result. An additional 25% increase in the metallicity term between the LMC and SMC comes from the decrease in the metallicity difference between the Clouds between Romaniello et al. (2008) used by OW22 and Romaniello et al. (2022) used here.

##### 5.5. Comparison between empirical estimates and theoretical predictions

While empirical estimates of the metallicity term of the PL relation have become more precise due to better parallaxes (Gaia Collaboration et al. 2021), reddening estimates, Cepheid photometry, and knowledge of Cloud geometry, they may appear to conflict with earlier pre-

<sup>2</sup> The  $+18 \mu\text{as}$  Gaia offset for bright objects proposed by OW22 conflicts with the  $\sim -15 \mu\text{as}$  mean of the measurements external to Gaia as summarized by Lindegren et al. (2021) and shown in Figure 1 by Li et al. (2022). This offset also makes Cepheids in the OW22 fainter by 0.074 mag, the Clouds closer by that amount and raises the local Hubble constant and its present tension by  $\sim 3.5\%$  without a metallicity term. In contrast, the metallicity term between the Clouds and MW presented here rather than a large, positive Gaia offset provides the consistency between the Gaia and DEB distances as they are the same size and direction.

<sup>3</sup> For the MW NIR, OW22 photometry is from Welch et al. (1984), Laney & Stobie (1992), Barnes et al. (1997) whereas ours is from Monson & Pierce (2011) with the latter having twice as many Cepheids and better calibration. For MW reddenings, OW22 uses the Fernie et al. (1995) database, a literature compilation of photoelectric photometry from uncommon bandpasses with a mean era of the 1980's and the Cardelli et al. (1989) reddening law, products that have not benefitted from the modern wide-field studies from Pan-STARRS and SDSS like Bayestar Green et al. (2019). For the LMC NIR data, OW22 uses 92 Cepheids from Persson et al. (2004) whereas this study augments that with  $> 750$  Cepheids from Macri et al. (2015). For the SMC NIR data, OW22 uses data from Laney & Stobie (1986), Welch et al. (1984) and Storm et al. (2004), whereas we use a larger sample from Ripepi et al. (2016) and Kato et al. (2007).

**Table 6.** Main improvements and updates between Breuval et al. (2021) and the present analysis.

	Breuval et al. (2021)	Present work
Filters:	$V, I, J, H, K$	$V, I, J, H, K$ <i>Gaia</i> $G, BP, RP$ <i>Spitzer</i> [3.6], [4.5]
Wesenheit indices:	$W_{VI}, W_{JK}$	$W_{VI}, W_{JK}$ $W_{VK}, W_H$ (HST), $W_G$ (Gaia)
Reddening law:	$A_\lambda/A_V$ from Cardelli et al. (1989)	$A_\lambda/A_V$ from Wang & Chen (2019) + uncertainties on $A_\lambda/A_V$ values + uncertainties on $R_V$ ( $3.1 \pm 0.1$ )
<i>Gaia</i> EDR3 parallax ZP:	Lindegren et al. (2021) $\varpi = \varpi_0 - ZP_{L21}$	Lindegren et al. (2021) $\varpi = \varpi_0 - (ZP_{L21} + 0.014 \mu\text{as})$
LMC metallicity:	$[\text{Fe}/\text{H}] = -0.34 \pm 0.06$ dex (Gieren et al. 2018)	$[\text{Fe}/\text{H}] = -0.407 \pm 0.020$ dex (Romaniello et al. 2022)
Reddening for MW Cepheids:	A13, K08, LC07, S07, A12, F95	(a) Bayestar dust map (Green et al. 2019) (b) Period-color relation (Riess et al. 2022) (c) SPIPS method (Trahin et al. 2021)
Reddening for LMC and SMC Cepheids:	Górski et al. (2020) reddening maps	Skowron et al. (2021) reddening maps
$V, I$ photometry for LMC Cepheids	OGLE-IV (Soszyński et al. 2015)	OGLE-IV (Soszyński et al. 2015) + Shallow Survey (Ulaczyk et al. 2013)

**References:** (A13): Anderson et al. (2013), (K08): Kovtyukh et al. (2008), (LC07): Laney & Caldwell (2007), (S07): Sziládi et al. (2007), (A12): Acharova et al. (2012), (F95): Fernie et al. (1995).

dictions from the theory (Bono et al. 1999, 2008; Caputo et al. 2000; Marconi et al. 2005). However, these early models also often combined simultaneous variations of the iron and helium content, factors which according to those models run counter to each other and which does not provide a standard reference for the value of  $\gamma$ .

More recently, Anderson et al. (2016) adopted the Geneva stellar evolution models by Georgy et al. (2013) that include the effects of stellar shellular rotation. They predicted the PL relation in  $V, H, W_{VI}$  and  $W_H$  for three different metal abundances ( $Z = 0.014, 0.006, \text{ and } 0.002$ , selected to match the MW, LMC and SMC Cepheids mean metallicity, respectively) and separately on the red and blue edge of the instability strip. We averaged the PL intercepts  $\beta$  listed in Table 2 of Anderson et al. (2016) on both edges for the second crossing of the instability strip, and represented them with  $[\text{Fe}/\text{H}]$  on Fig. 6. We find that the variation of these intercepts with  $[\text{Fe}/\text{H}]$  yield a negative metallicity effect of  $\gamma \sim -0.2$  mag/dex across the optical and NIR, consistent with our present results. While additional theoretical studies are warranted, the agreement found here is quite promising.

## 6. CONCLUSIONS AND PERSPECTIVES

The results by Breuval et al. (2021) suggested a possible dependence of  $\gamma$  with wavelength, but were based on only five filters. To explore this question, we extended the wavelength range by including new mid-IR (*Spitzer*) and optical (*Gaia*) bands. We were able to take this analysis one step further by improving the technique and updating the data wherever it was possible. All the improvements included in this study are listed in Table 6 and compared with the previous Breuval et al. (2021) paper. We note that the uncertainties on the  $\gamma$  terms presented in this paper are not significantly smaller compared with previous analysis, despite the several improvements included: this is because we now include the uncertainties on the reddening law and on the  $R_V$  values, which were not considered previously.

We report values of the metallicity effect on the Cepheid PL relation in 10 filters from  $0.5 \mu\text{m}$  to  $4.5 \mu\text{m}$  and in 5 Wesenheit indices, including the HST based Wesenheit index  $W_H$  used for the SH0ES distance ladder (Riess et al. 2022). We obtain a negative  $\gamma$  term in all bands, meaning that metal-rich Cepheids are brighter than metal-poor ones, in agreement with all recent em-

pirical studies. We find a globally uniform value of  $\gamma$  from optical to mid-IR filters, showing that the main influence of metallicity on Cepheids is in their brightness rather than color.

While our results are largely consistent with recent measurements, we track differences in two studies, (Wielgórski et al. 2017; Owens et al. 2022) that employ the SMC to a depth effect. Correcting for the geometry and limiting the radius to the SMC core is shown to narrow the distance range resulting in a sample insured to be at the same distance as the DEBs that also produces a metallicity term on the same trend line as seen between the MW and LMC.

Comparing Cepheids over a sufficiently large metallicity range still requires to combine different samples of Cepheids located in several galaxies, having different distances, photometric systems, dust distribution and properties (e.g. reddening law), which implies large systematic uncertainties. In the near future, it should be possible to reduce the impact of these systematics and to increase the precision of the  $\gamma$  term thanks to the 4th *Gaia* data release. Ideally, these new distance measurements will have to be combined with consistent metallicity estimates of all Milky Way Cepheids obtained in a single system, spanning a wide range of abundances. In this sense, improvements are also expected from the use of recently published (Ripepi et al. 2021; Romaniello et al. 2022; da Silva et al. 2022) and upcoming abundance catalogs for MW, LMC and

SMC Cepheids, which should again help to calibrate the metallicity effect with a better accuracy.

#### ACKNOWLEDGEMENTS

L.B. is grateful to C. A. L. Bailer Jones, F. Arénou, B. Trahin, R. I. Anderson and A. Mérand for fruitful discussions that helped to improve this paper. We wish to thank L. M. Macri for providing the photometric transformations to the 2MASS system. The research leading to these results has received funding from the European Research Council (ERC) under the European Union’s Horizon 2020 research and innovation program (projects CepBin, grant agreement 695099, and UniverScale, grant agreement 951549). This work has made use of data from the European Space Agency (ESA) mission *Gaia* (<http://www.cosmos.esa.int/gaia>), processed by the *Gaia* Data Processing and Analysis Consortium (DPAC, <http://www.cosmos.esa.int/web/gaia/dpac/consortium>). Funding for the DPAC has been provided by national institutions, in particular the institutions participating in the *Gaia* Multilateral Agreement. This research made use of *Astropy*7, a community-developed core Python package for Astronomy (Astropy Collaboration et al. 2018). We used the SIMBAD and VIZIER databases and catalog access tool at the CDS, Strasbourg (France), and NASA’s Astrophysics Data System Bibliographic Services.

#### REFERENCES

- Acharova, I. A., Mishurov, Y. N., & Kovtyukh, V. V. 2012, *MNRAS*, 420, 1590
- Anderson, R. I., Eyer, L., & Mowlavi, N. 2013, *MNRAS*, 434, 2238
- Anderson, R. I., Saio, H., Ekström, S., Georgy, C., & Meynet, G. 2016, *A&A*, 591, A8
- Astropy Collaboration, Price-Whelan, A. M., Sipőcz, B. M., et al. 2018, *AJ*, 156, 123
- Bailer-Jones, C. A. L., Rybizki, J., Foesneanu, M., Demleitner, M., & Andrae, R. 2021, *AJ*, 161, 147
- Barnes, T. G., I., Fernley, J. A., Frueh, M. L., et al. 1997, *Publications of the Astronomical Society of the Pacific*, 109, 645
- Berdnikov, L. N. 2008, *VizieR Online Data Catalog*, 2285, 0
- Bono, G., Caputo, F., Castellani, V., & Marconi, M. 1999, *ApJ*, 512, 711
- Bono, G., Caputo, F., Fiorentino, G., Marconi, M., & Musella, I. 2008, *ApJ*, 684, 102
- Breival, L., Kervella, P., Wielgórski, P., et al. 2021, *ApJ*, 913, 38
- Caputo, F., Marconi, M., Musella, I., & Santolamazza, P. 2000, *A&A*, 359, 1059
- Cardelli, J. A., Clayton, G. C., & Mathis, J. S. 1989, *ApJ*, 345, 245
- Clementini, G., Ripepi, V., Molinaro, R., et al. 2019, *A&A*, 622, A60
- da Silva, R., Crestani, J., Bono, G., et al. 2022, arXiv e-prints, arXiv:2202.07945
- Di Valentino, E., Mena, O., Pan, S., et al. 2021, arXiv e-prints, arXiv:2103.01183
- Fernie, J. D., Evans, N. R., Beattie, B., & Seager, S. 1995, *Information Bulletin on Variable Stars*, 4148
- Fitzpatrick, E. L., Massa, D., Gordon, K. D., Bohlin, R., & Clayton, G. C. 2019, *ApJ*, 886, 108
- Freedman, W. L., & Madore, B. F. 2011, *ApJ*, 734, 46

- Freedman, W. L., Madore, B. F., Gibson, B. K., et al. 2001, *ApJ*, 553, 47
- Freedman, W. L., Madore, B. F., Scowcroft, V., et al. 2011, *AJ*, 142, 192
- Gaia Collaboration, Brown, A. G. A., Vallenari, A., et al. 2021, *A&A*, 649, A1
- Genovali, K., Lemasle, B., Bono, G., et al. 2014, *A&A*, 566, A37
- Genovali, K., Lemasle, B., da Silva, R., et al. 2015, *A&A*, 580, A17
- Georgy, C., Ekström, S., Granada, A., et al. 2013, *A&A*, 553, A24
- Gieren, W., Storm, J., Konorski, P., et al. 2018, *A&A*, 620, A99
- Gordon, K. D., Clayton, G. C., Misselt, K. A., Landolt, A. U., & Wolff, M. J. 2003, *ApJ*, 594, 279
- Górski, M., Zgirski, B., Pietrzyński, G., et al. 2020, *ApJ*, 889, 179
- Graczyk, D., Pietrzyński, G., Thompson, I. B., et al. 2014, *ApJ*, 780, 59
- . 2020, *ApJ*, 904, 13
- Green, G. M., Schlafly, E., Zucker, C., Speagle, J. S., & Finkbeiner, D. 2019, *ApJ*, 887, 93
- Groenewegen, M. A. T. 2013, *A&A*, 550, A70
- . 2018, *A&A*, 619, A8
- Jacyszyn-Dobrzeńicka, A. M., Skowron, D. M., Mróz, P., et al. 2016, *AcA*, 66, 149
- Kato, D., Nagashima, C., Nagayama, T., et al. 2007, *PASJ*, 59, 615
- Kennicutt, Robert C., J., Stetson, P. B., Saha, A., et al. 1998, *ApJ*, 498, 181
- Kovtyukh, V. V., Soubiran, C., Luck, R. E., et al. 2008, *MNRAS*, 389, 1336
- Laney, C. D., & Caldwell, J. A. R. 2007, *MNRAS*, 377, 147
- Laney, C. D., & Stobie, R. S. 1986, *MNRAS*, 222, 449
- . 1992, *Astronomy and Astrophysics Supplement Series*, 93, 93
- Leavitt, H. S., & Pickering, E. C. 1912, *Harvard College Observatory Circular*, 173, 1
- Li, S., Casertano, S., & Riess, A. G. 2022, *arXiv e-prints*, [arXiv:2202.11110](https://arxiv.org/abs/2202.11110)
- Lindegren, L., Bastian, U., Biermann, M., et al. 2021, *A&A*, 649, A4
- Macri, L. M., Ngeow, C.-C., Kanbur, S. M., Mahzooni, S., & Smitka, M. T. 2015, *AJ*, 149, 117
- Macri, L. M., Stanek, K. Z., Bersier, D., Greenhill, L. J., & Reid, M. J. 2006, *ApJ*, 652, 1133
- Madore, B. F. 1982, *ApJ*, 253, 575
- Marconi, M., Musella, I., & Fiorentino, G. 2005, *ApJ*, 632, 590
- Marengo, M., Evans, N. R., Barmby, P., et al. 2010, *ApJ*, 725, 2392
- Mérand, A., Kervella, P., Breielfelder, J., et al. 2015, *A&A*, 584, A80
- Monson, A. J., Freedman, W. L., Madore, B. F., et al. 2012, *ApJ*, 759, 146
- Monson, A. J., & Pierce, M. J. 2011, *ApJS*, 193, 12
- Nidever, D. L., Majewski, S. R., & Butler Burton, W. 2008, *ApJ*, 679, 432
- Owens, K. A., Freedman, W. L., Madore, B. F., & Lee, A. J. 2022, *ApJ*, 927, 8, doi: [10.3847/1538-4357/ac479e](https://doi.org/10.3847/1538-4357/ac479e)
- Persson, S. E., Madore, B. F., Krzemiński, W., et al. 2004, *AJ*, 128, 2239
- Pietrzyński, G., Graczyk, D., Gieren, W., et al. 2013, *Nature*, 495, 76
- Pietrzyński, G., Graczyk, D., Gallenne, A., et al. 2019, *Nature*, 567, 200
- Planck Collaboration, Aghanim, N., Akrami, Y., et al. 2020, *A&A*, 641, A6
- Riess, A. G., Casertano, S., Yuan, W., et al. 2021, *ApJL*, 908, L6
- Riess, A. G., Casertano, S., Yuan, W., Macri, L. M., & Scolnic, D. 2019, *ApJ*, 876, 85
- Riess, A. G., Macri, L., Casertano, S., et al. 2009, *ApJ*, 699, 539
- . 2011, *ApJ*, 730, 119
- Riess, A. G., Macri, L. M., Hoffmann, S. L., et al. 2016, *ApJ*, 826, 56
- Riess, A. G., Yuan, W., Macri, L. M., et al. 2022, *arXiv e-prints*, [arXiv:2112.04510](https://arxiv.org/abs/2112.04510)
- Ripepi, V., Molinaro, R., Musella, I., et al. 2019, *A&A*, 625, A14
- Ripepi, V., Marconi, M., Moretti, M. I., et al. 2016, *ApJS*, 224, 21
- Ripepi, V., Catanzaro, G., Molinaro, R., et al. 2020, *A&A*, 642, A230
- . 2021, *MNRAS*
- Ripepi, V., Catanzaro, G., Clementini, G., et al. 2022, *A&A*, 659, A167
- Romaniello, M., Primas, F., Mottini, M., et al. 2008, *A&A*, 488, 731
- Romaniello, M., Riess, A., Mancino, S., et al. 2022, *A&A*, 658, A29
- Sakai, S., Ferrarese, L., Kennicutt, Robert C., J., & Saha, A. 2004, *ApJ*, 608, 42
- Scowcroft, V., Bersier, D., Mould, J. R., & Wood, P. R. 2009, *MNRAS*, 396, 1287
- Scowcroft, V., Freedman, W. L., Madore, B. F., et al. 2016, *ApJ*, 816, 49
- . 2011, *ApJ*, 743, 76

- Skowron, D. M., Skowron, J., Udalski, A., et al. 2021, ApJS, 252, 23
- Soszyński, I., Udalski, A., Szymański, M. K., et al. 2015, AcA, 65, 297
- Storm, J., Carney, B. W., Gieren, W. P., et al. 2004, A&A, 415, 531
- Storm, J., Gieren, W., Fouqué, P., et al. 2011a, A&A, 534, A95
- . 2011b, A&A, 534, A94
- Sziládi, K., Vinkó, J., Poretti, E., Szabados, L., & Kun, M. 2007, A&A, 473, 579
- Trahin, B., Breuval, L., Kervella, P., et al. 2021, A&A, 656, A102
- Ulaczyk, K., Szymański, M. K., Udalski, A., et al. 2013, AcA, 63, 159
- Wang, S., & Chen, X. 2019, ApJ, 877, 116
- Watson, C. L., Henden, A. A., & Price, A. 2006, Society for Astronomical Sciences Annual Symposium, 25, 47
- Welch, D. L., Wieland, F., McAlary, C. W., et al. 1984, ApJS, 54, 547
- Wielgórski, P., Pietrzyński, G., Gieren, W., et al. 2017, ApJ, 842, 116
- Zinn, J. C. 2021, AJ, 161, 214